Capacitively Coupled Electrical Impedance Tomography (CCEIT) for Brain Imaging

Y. D. Jiang* and M. Soleimani

***Abstract*—Electrical impedance tomography (EIT) is considered as a potential candidate for brain stroke imaging due to its compactness and potential use in bedside and in emergency settings. The electrode-skin contact impedance and low conductivity of skull pose some major practical challenges in EIT head imaging. This work studies the use of capacitively coupled electrical impedance tomography (CCEIT), a new contactless EIT technique for brain imaging. CCEIT uses voltage excitation without direct contact with the skin, as oppose to direct current injection in EIT. Because the safety issue of a new technique should be strictly treated, simulation work based on a simplified head model was carried out to investigate the safety aspects of CCEIT. By comparing with standard EIT excited by a typical safe current level used in brain imaging, the safe excitation reference of CCEIT is obtained. This is done by comparing the maximum level of internal electrical fields of EIT and CCEIT and hence internal current density. Simulation results provide useful knowledge concerning the level of excitation signal in CCEIT and also a critical comparison with traditional EIT. Experiments were carried out with a twelve-electrode CCEIT phantom to study its performance for stroke imaging. Experimental results show the feasibility and potential of CCEIT on stroke imaging with an anomaly diameter resolution of 10 mm, which is 1/18 of the phantom diameter showing small volume stroke could be detected. This is achieved by an excitation voltage of 1V, much lower than safe level of excitation, with possibility of even better performance when higher level of excitation voltages is used.**

***Index Terms*—Capacitively coupled electrical impedance tomography (CCEIT), stroke imaging, safety issue, multi-frequency time-difference imaging**

I. Introduction

STROCK carries a high morbidity rate and is now the second leading cause of death worldwide after heart disease [1-3]. Because the type, position and size information of the stroke plays a vital role for appropriate treatment, accurate diagnosis is of significant importance [2-8]. For hemorrhagic stroke, it requires urgent treatment with a consequent need for quick and accurate diagnosis [9-10]. When a stroke is occurred, treatments should be given to the patients within the first few hours after the bleeding position is located and the size information of bleeding area can provide important reference for doctors during treatment. In current clinical diagnosis of stroke, computed tomography (CT) and magnetic resonance imaging (MRI) are two main methods to provide accurate results [11-12]. However, the devices of CT and MRI are expensive and in large volume, so it is impossible to arrange urgent CT or MRI scanning in patients' home, ambulance or primary health care units. Thus there is a clear clinical need for new portable devices which can rapidly provide accurate imaging results without waiting for hospital admission of a CT/MRI scanning.

Electrical impedance tomography (EIT) has been widely studied and applied in medical applications since proposed in 1980s. Due to various advantages such as safe, fast, cheap and portable, it is now a very promising non-invasive technique in stroke imaging [2-10]. One of the most important challenges of medical EIT is the electrode-skin contact impedance, which is usually high and quite variable due to body surface condition and body movement. Besides, research results show that this contact impedance is sensitive to properties of the contact layer [13]. So, the contact impedance is a crucial accuracy-limiting factor. In the past decades, many research works have been undertaken to overcome the contact impedance [4, 14-16]. However, most of them focus on modeling, calculating and reducing the contact impedance, not completely eliminating it.

In 2013, a new kind of EIT technique termed capacitively coupled electrical resistance tomography (CCERT) was proposed for industrial application to implement contactless conductivity imaging [17-18]. Based on the capacitively coupled contactless conductivity detection (C^4D) technique, this capacitively coupled EIT technique (CCEIT) doesn't require electrodes to contact directly with the conductive medium, so it can overcome many negative sides of contact measurement.

Current CCEIT-related research works mainly focus on industrial applications (parameter measurement of multi-phase flow), the work in [19] is the first attempt to introduce CCEIT to biomedical and biomaterial applications and it shows the potential of this technique in general biomedical application. The safety issue and resolution aspects of CCEIT for further medical study have not been studied. Besides, specified medical applications of this technique, like head imaging and lung imaging, still need more targeted research.

This work for the first time considers the safety issue of

Y. D. Jiang is with the Engineering Tomography Laboratory (ETL), Department of Electronic and Electrical Engineering, University of Bath, Bath, BA2 7AY, UK and the State Key Laboratory of Industrial Control Technology, College of Control Science and Engineering, Zhejiang University, Hangzhou, 310027, China (e-mail: jiangyandan123@163.com).

M. Soleimani is with the Engineering Tomography Laboratory (ETL), Department of Electronic and Electrical Engineering, University of Bath, Bath, BA2 7AY, UK (e-mail: m.soleimani@bath.ac.uk).

CCEIT and studies its resolution specifically on stroke imaging. With a simplified head model, simulation work was carried out to investigate the electrical field distribution of CCEIT inside the sensing area. Meanwhile, the safety issue of CCEIT is discussed in terms of the maximum current density when compared with traditional EIT. Experiments were carried out to obtain resistance measurements over a wide frequency range. Multi-frequency time-difference imaging was implemented by Gaussian-Newton based Tikhonov regularization algorithm. Imaging results show the resolution of this contactless technique for stroke imaging. The basic measurement principle is described in Section II. Methods of forward modeling and image reconstruction are introduced in Section III. Excitation voltage of CCEIT within safe level, including the influence of frequency and thickness of the insulation layer of CCEIT, is presented in Section IV. Experimental setup and experimental results are respectively shown in Section V and Section VI.

II. Measurement Principle

Fig. 1 shows the measurement principle of a twelve-electrode CCEIT phantom for head imaging. In this work, an anatomically accurate but simplified head model is adopted [9], which includes the outer layer and the brain layer for healthy head and an additional stroke layer for stroke patients. Fig. 1(a) shows the construction of the CCEIT sensing region, which mainly includes four layers, the insulation layer, the outer layer, the brain layer and the stroke layer. The twelve electrodes are mounted equidistantly outside the insulation layer. For any two electrodes, the electrodes, the insulation layer and the conductive layers form two coupling capacitances (C_1 and C_2). The three conductive layers of the head can be equivalent to impedance Z_x. So, the equivalent circuit of any electrode pair can be simplified as two coupling capacitances in series with the impedance Z_x, as shown in Fig. 1(b). It is obvious that the insulation layer makes the contactless measurement possible.

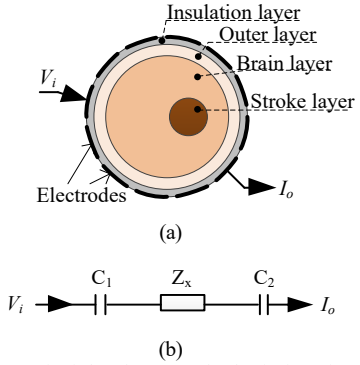

Fig. 1. Measurement principle of CCEIT for brain imaging. (a) Construction of the sensing area. (b) Equivalent circuit of an electrode pair.

The whole impedance Z of an electrode pair is

$$Z = Z_x + \frac{1}{j\omega C_c} = Z_x - j\frac{1}{2\pi f C_c} \quad (1)$$

where, ω and f are respectively the angular frequency and frequency of the excitation signal. C_c is the whole equivalent capacitance of the two coupling capacitances C_1 and C_2.

When an AC voltage source V_i is applied to the excitation electrode, a current I_o which reflects the impedance of the sensing area between the measurement electrode pair can be obtained on the detection electrode. In this work, the resistance component of the impedance is used for conductivity imaging. During measurement, other electrodes are kept at floating potential. For a twelve-electrode setup, 66 independent measurements can be obtained in a whole measurement cycle. First, electrode 1 and 2 are selected as the measurement electrode pair. Then, electrode 1 is still the excitation electrode and the detection electrode is changed to electrode 3~12 one by one. Next, changing the excitation electrode to electrode 2 and the detection electrode to electrode 3~12 by turn. Go on until electrode 11 and 12 are selected as the measurement pair.

III. Forward Modeling and Image Reconstruction

There are basically two essential problems to be solved in EIT, one is the forward problem and the other is the inverse problem [20-21]. Forward problem is to obtain the boundary measurements with known conductivity distribution inside the sensing area. While inverse problem is reconstructing the internal conductivity distribution based on known boundary measurements and a pre-calculated sensitivity matrix. This section describes the used methods of forward modeling, sensitivity matrix calculation and image reconstruction of CCEIT.

A. Forward modeling

As shown in Fig. 2, there are three subdomains for the healthy CCEIT head model, including the insulation layer (conductivity σ_I = 0 S/m, outer diameter (OD) = 184 mm), the outer layer (σ_O = 0.06 S/m, OD = 180 mm) with low conductivity which represents the low-conductive layers of human head (i.e. the scalp and skull) and the brain layer (σ_B = 0.15 S/m, OD = 170 mm) which represents the higher conductive brain layer inside the human head. The relative permittivity of the insulation layer is set to 3 and those of the other layers are set to 80.

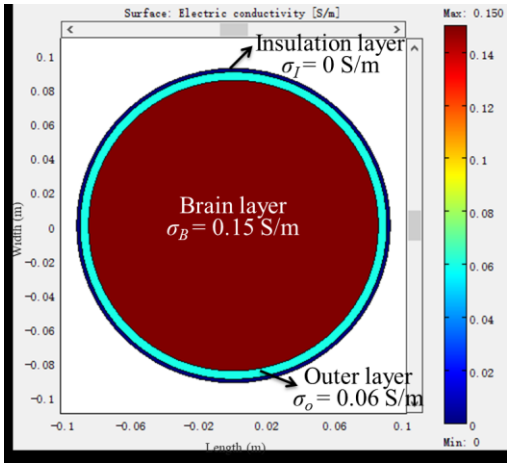

Fig. 2. Subdomain setup with simplified healthy CCEIT head model.

For general excitation frequency, the wavelength of the excitation signal is much larger than the size of the sensing area. So, the sensing area of CCEIT can be regarded as a quasi-static electric field. Besides, the fringe effect caused by the finite

electrode length is neglected to simplify the model. Therefore, the model of the CCEIT sensing area can be described by the following equation [18, 22]

$$\nabla \cdot ((\sigma(x,y) + j\omega\varepsilon(x,y))\nabla\varphi(x,y)) = 0 \quad (x,y) \subseteq \Omega \tag{2}$$

where, $\sigma(x, y)$, $\varepsilon(x, y)$ and $\varphi(x, y)$ are the spatial conductivity, permittivity and potential distributions. $\omega=2\pi f$ is the angular frequency of the excitation AC voltage source. f is the frequency of the AC voltage source. Ω is the sensing area. The boundary conditions of the model in (2) are

$$\begin{cases} \varphi_a(x,y) = V & (x,y) \subseteq \Gamma_a \\ \varphi_b(x,y) = 0 & (x,y) \subseteq \Gamma_b \\ \partial\varphi_c(x,y)/\partial\hat{n} = 0 & (x,y) \subseteq \Gamma_c, (c \neq a,b) \end{cases} \tag{3}$$

where, V is the amplitude of the excitation AC voltage source. Γ_1, Γ_2, Γ_3, …, Γ_{12} represent the spatial locations of the 12 electrodes. $\hat{n}$ denotes the outward unit normal vector. a, b and c are the indexes of the excitation electrode, the detection electrode and the floating electrodes, respectively.

B. Sensitivity matrix

Based on the finite element method (FEM), simulation is carried out by software (Comsol Multiphysics and MATLAB) and the sensitivity matrix is calculated. Sensitivity matrix reveals the relationship between the resistance measurement and the internal conductivity distribution. The sensing area is meshed into 864 triangle elements, as shown in Fig. 3. Then the sensitivity matrix is defined as

$$S = [s_{ij}] \tag{4}$$

$$s_{ij} = \frac{\partial R}{\partial \sigma} \approx \frac{R_i^j - R_i^0}{\sigma^1 - \sigma^0} \tag{5}$$

where, s_{ij} is the sensitivity of the jth element under the ith electrode pair (i.e. the ith independent measurement), i=1, 2, …, 66, j=1, 2, …, 864. R is the resistance measurement and σ is the conductivity distribution. R_i^0 represent the ith resistance measurement when the region of interest is full of healthy tissue/background ($\sigma = \sigma^0$) and $R_i{}^j$ is the ith resistance measurement when the dielectric parameters of the jth element changes from healthy tissue to diseased tissue/anomaly ($\sigma = \sigma^1$) and the remaining elements are still kept at the dielectric parameters of the healthy tissue ($\sigma = \sigma^0$).

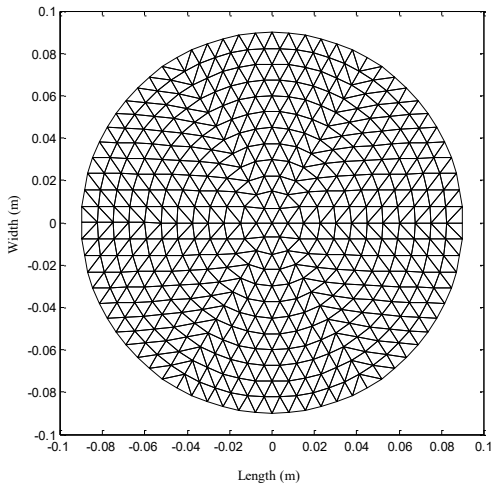

Fig. 3. Finite element mesh of the simulation model.

C. Image reconstruction

Similar with the inverse problem of traditional EIT, image reconstruction of CCEIT can be described as solving the following equation [23]

$$\Delta R = S\Delta\sigma \tag{6}$$

where, ΔR is the time-difference resistance projection vector and $\Delta\sigma$ is the relative conductivity distribution to be reconstructed.

The inverse problem is badly ill-posed, so the solution can not be obtained by directly calculating the inverse of the sensitivity matrix [24-25]. In this work, the image reconstruction is implemented by the Gaussian-Newton based Tikhonov regularization method. First, an initial solution is obtained by the one-step Tikhonov method. Then, with the initial solution, Gaussian-Newton iteration method is introduced to determine the final solution. Tikhonov regularization method adds a trade-off between the accurate solution to the problem and the norm of the solution [25-27]. It is governed by the following objective function

$$\Delta\sigma_\lambda = \arg\min_{\Delta\sigma} \left\| S\Delta\sigma - \Delta R \right\|^2 + \lambda^2 \left\| \Delta\sigma \right\|^2 \tag{7}$$

where, λ is the regularization parameter that controls the amount of regularization. The corresponding solution is

$$\Delta\sigma_\lambda = (S^{\mathrm{T}}S + \lambda^2 I_n)^{-1} S^{\mathrm{T}}\Delta R \tag{8}$$

where, I_n is the identity matrix used in the Tikhonov method.

IV. Excitation Level in CCEIT

Safety issue is critical in medical applications as it is closely related to human lives. Before practical vivo application in future, the safety of a new technique should be studied to make sure it is safe enough and make the reference level of safe excitation signal clear. So, the signal strength inside the sensing area of CCEIT is investigated by comparing with that of traditional EIT. This will also help to put in prospect the expected imaging performance with the same level of electric field distribution against standard EIT.

A. Simulation setup and electric field distribution

According to previous medical EIT research, the standard electrical current injected into the object is typically 1 mA at 50 kHz, which is safe enough for medical application [6]. So, based on this standard excited EIT head model, the safe excitation level of CCEIT head model is investigated. In this work, the maximum total current density (norm) is introduced as a quantitative index to compare the two. The reference of safe excitation level for CCEIT is determined when the maximum total current density inside the CCEIT head model is the same as that inside the EIT head model. The subdomain setup of healthy CCEIT head model has been shown in Fig. 2.

Fig.4 shows the boundary setups of the EIT and the CCEIT in simulation. Different colors indicate different boundary conditions. Sky blue represents the excitation electrode, pink means the detection electrode and green indicates the floating electrodes. The colors are indicated by the software after the boundary conditions are set.

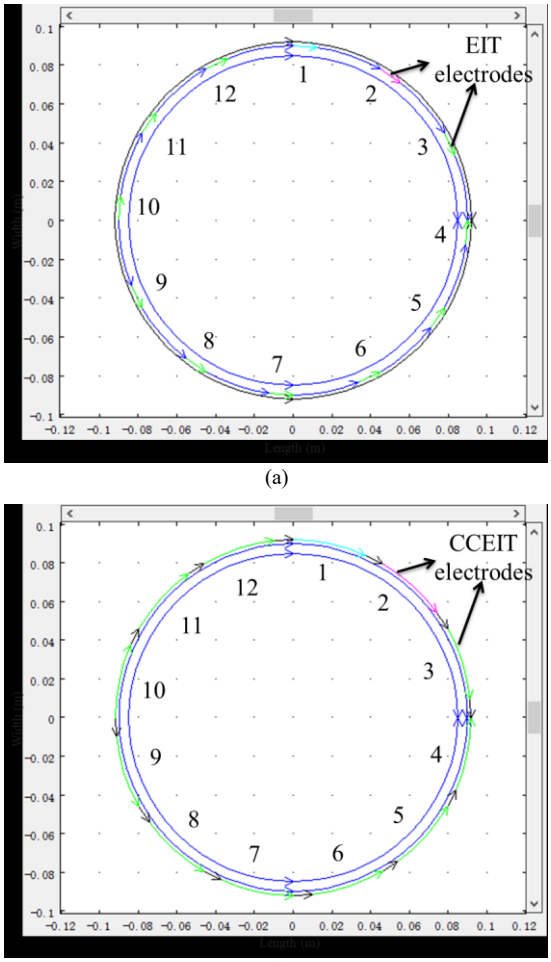

(a)

(b)

Fig. 4. Boundary setup. (a) EIT with adjacent current excitation (electrode angle is 8°). (b) CCEIT with one electrode voltage excitation and the adjacent electrode detection (electrode angle is 24°).

In EIT setup, the electrodes are distributed equidistantly outside the outer layer of the head model, in direct contact with the low conductive layer of the head model, as shown in Fig. 4(a). For traditional EIT, electrodes are usually small to ensure better sensitivity distribution in the sensing area, so small EIT electrodes are designed with an electrode angle of 8°. Besides, the most commonly used adjacent excitation pattern of EIT is introduced, which injects a standard AC current (1 mA, 50 kHz) into an adjacent electrode pair. In CCEIT setup, electrodes are mounted outside the insulation layer, which prevents direct contact between the electrodes and the skin, as shown in Fig. 4(b). According to previous simulation work of CCEIT, larger electrode angle contributes to better measurement performance [18]. But with larger electrode angle, the gap between electrodes will be reduced, which results in higher parasitic capacitance between electrodes. So, after trade-off consideration, the electrode angle of CCEIT is set to 24°. During measurement, an AC voltage source is applied to the excitation electrode of CCEIT and measurement is obtained at the adjacent detection electrode.

According to the simulation results of traditional EIT based on the above setup, a safe current input of EIT with 1 mA at 50 kHz can produce an electric field with the maximum total current density (norm) of 7.584 A/m^2. So, the safe excitation voltage of the CCEIT is determined by producing an electric field with the same maximum total current density (norm).

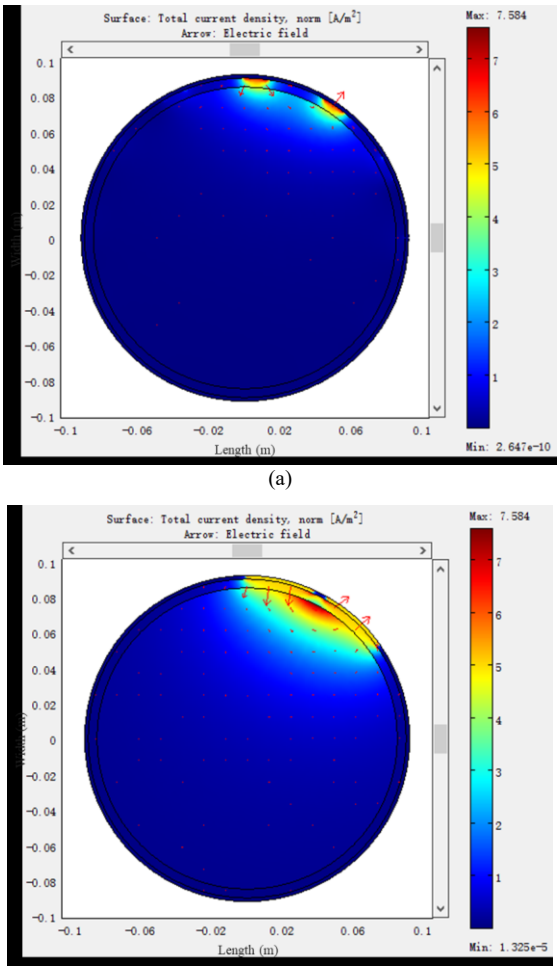

(a)

(b)

Fig. 5. Electric field distribution and total current density distribution of healthy head model. (a) EIT. (b) CCEIT.

Fig. 5 shows the electric field distribution and the total current density (norm) distribution in the sensing area of the simulated EIT and CCEIT head model. It is clear that the strength of the electric field mainly concentrated near the excitation electrode(s). For the EIT model, the highest total current density positioned at the excitation electrodes. While for the CCEIT model, the highest total current density positioned in the brain layer between the selected electrode pair.

B. Stroke-introduced CCEIT head model

In order to investigate the influence of the stroke on the electrical field distribution, another head model which introduces an additional hemorrhagic stroke layer (σ_S= 0.6 S/m, OD = 40 mm) for stroke patients is established, as shown in Fig. 6.

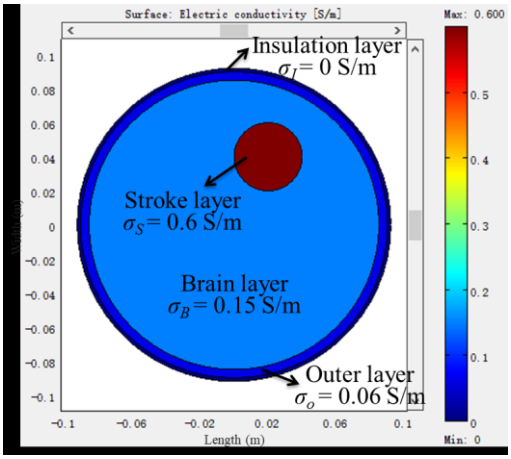

Fig. 6. Subdomain setup of stroke-introduced CCEIT head model.

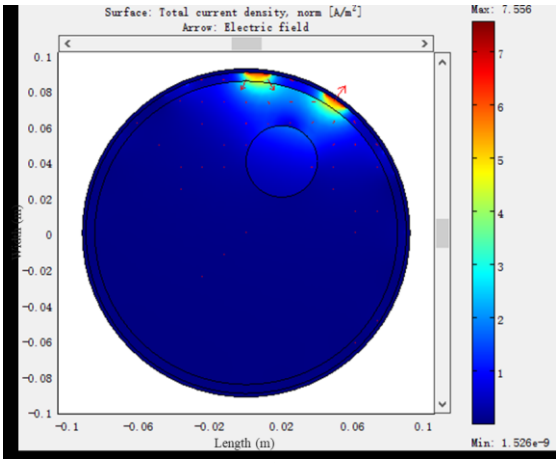

(a)

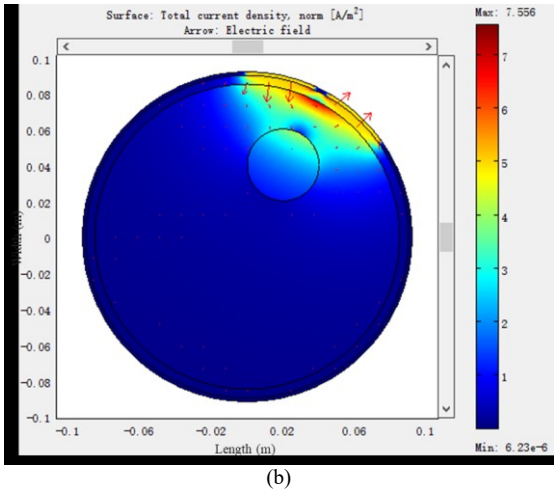

(b)

Fig. 7. Electric field distribution and total current density distribution of stroke-introduced head model. (a) EIT. (b) CCEIT.

Fig. 7 shows the electric field distribution and the total current density (norm) distribution in the sensing area of stroke-introduced EIT and CCEIT head model. Similarly, electric field near the excitation electrode(s) area is much stronger than other area. However, as the conductivity of the hemorrhagic stroke is higher than the brain layer, many electric field lines are attracted by the stroke area and the current density in the stroke area becomes higher than that in the same area in Fig. 5. With the stroke-introduced setup, a safe input of EIT with 1 mA at 50 kHz can produce a corresponding electric field with the maximum total current density (norm) of 7.556 A/m^2, which is a bit lower than that with healthy head model.

C. Influence of frequency

It is obvious from (2) that frequency has a big influence on the electric field. So, for either traditional EIT or the new CCEIT, when it comes to the safe excitation current/voltage, the frequency should be clearly pointed out. Take the electric field of traditional EIT excited by the safe current level of 1 mA at 50 kHz as a standard, the equivalent excitation voltages of CCEIT at different frequencies are determined by simulation to produce an electric field with the same maximum total current density (norm). The setups are shown in Fig. 4.

Based on previous research results, the working frequency of CCEIT should be a bit high (usually 500 kHz or higher) to ensure good performance because of the coupling capacitances. For the healthy head model, in order to obtain the same maximum total current density as EIT with 1 mA current input at 50 kHz, the CCEIT allows inputting a voltage of 239.845 V, 119.986 V, 24.345 V, 12.399 V and 8.408 V at 500 kHz, 1 MHz, 5 MHz, 10 MHz and 15 MHz, respectively. For the stroke-introduced head model, the allowed inputting voltages are slightly lower, which are 238.942 V, 119.543 V, 24.278 V, 12.357 V and 8.375 V at 500 kHz, 1 MHz, 5 MHz, 10 MHz and 15 MHz, respectively. These are the safe references of excitation level for CCEIT equivalent to the safe 1 mA excited medical EIT, based on the established head models. To double verify the data reliability (especially the allowed high voltage value at low frequency), more simulation work was carried out. Results show that the values of electric field strength (norm, V/m) and electric energy density (time average, J/m^3) at the first skin layer of the head (i.e. the outer layer) are similar for EIT excited by 1 mA at 50 kHz and CCEIT excited by 239.845 V at 500 kHz. That further verifies the obtained excitation references of CCEIT are reliable.

Fig. 8 shows the safe excitation voltages of CCEIT over a wide frequency range from 500 kHz to 15 MHz. As the frequency increases, the safe excitation voltage decreases. For practical application, the excitation voltage should be determined by the maximum frequency. Besides, when the voltage provided by the device is not high enough to ensure good signal-to-noise (SNR) ratio, increasing the working frequency within a totally safe range is also a good choice.

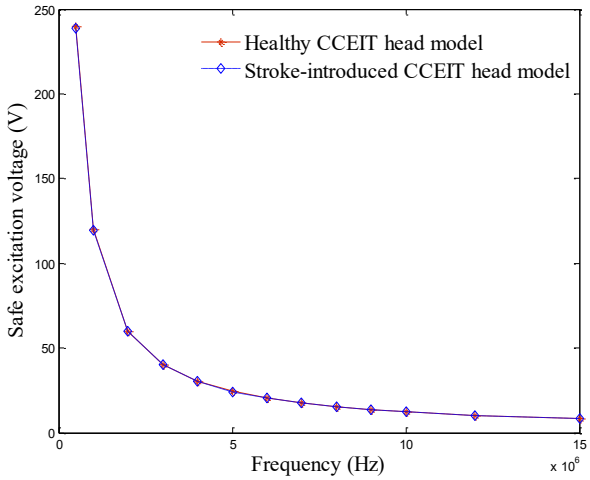

Fig. 8. Safe excitation voltages of CCEIT head imaging over a wide frequency range from 500 kHz to 15 MHz.

D. Influence of insulation thickness

The insulation layer of CCEIT is the key of contactless measurement, but it has big influence on signal strength. So, the relationship between the safe excitation voltage and the thickness of the insulation layer (insulation thickness) is also studied, based on the healthy CCEIT head model. Fig. 9 shows the safe excitation voltages of CCEIT at 15 MHz with different insulation thickness from 1 mm to 20 mm. The voltage shows an overall increasing trend when the insulation thickness goes up, which means the insulation layer weakens the signal strength. From the aspect of signal measurement, thinner insulation thickness is preferred.

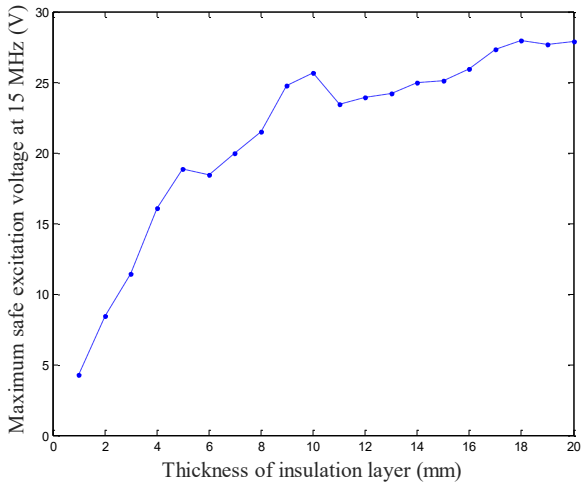

Fig. 9. Safe excitation voltages of CCEIT with insulation thickness from 1 mm to 20 mm.

V. Experimental Setup

Studies in phantoms represent a bridge between idealized computer simulations and clinical measurements where instrumentation noise is present but errors in modeling the electric fields are minimized [31]. In this work, a twelve-electrode CCEIT phantom was developed. The insulation pipe (wall of the tank), including the bottom of the tank, was produced by 3D printing with the material of polylactic acid (PLA). The electrodes were made from copper sheet. The electrode angle and length of electrodes were 24° and 50 mm. The inner and outer diameters of the insulation tank were 180 mm and 184 mm, respectively. Saline with the conductivity of 0.143 S/m was used to simulate the brain layer. The conductivity was measured by a conductivity meter (Jenway 4510) at the experimental temperature of 20.5 ℃ and the temperature was relatively stable during experiments. Four carrot samples with different diameters were used to simulate the stroke with different sizes, to show the resolution of the contactless CCEIT in stroke imaging. The diameters of the four samples were respectively 35 mm, 25 mm, 15 mm and 10 mm. In all the setups, the samples were located at the same place near the boundary for better comparison between them. The measurement system is shown in Fig. 10. An impedance analyzer (Keysight E4990A) was used to obtain resistance measurement. The sweep frequency and sweep points of the impedance analyzer were set to 200 kHz ~ 15 MHz and 201 points, which means 201 resistance measurements at 201 frequency points can be obtained for every measurement. The excitation voltage of the impedance analyzer was set to 1 V. A computer was used for image reconstruction.

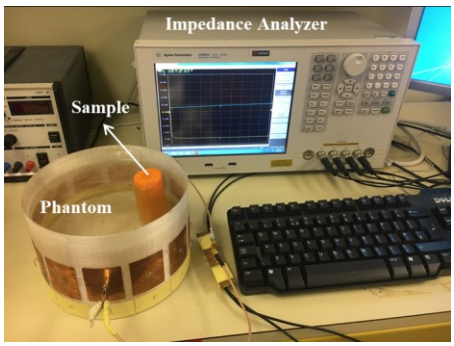

Fig. 10. Measurement system.

VI. Results and Discussion

A. Image reconstruction results

Fig. 11 ~ Fig. 14 show the image reconstruction results of the four carrot samples, respectively. Images obtained at 15 frequency points in a wide frequency range from 200 kHz to 15 MHz are listed. The accurate size and position of the samples are indicated by a circle with solid red line. The selection of λ in (8) is the key of Tikhonov regularization method. If λ is too large, then the solution is poorly resolved. If λ is too small, then the solution is too noisy. Many methods have been proposed to determine λ, such as the discrepancy principle, the L-curve method and the cross-validation method. The regularization parameter λ in this work is pre-determined by the L-curve method, which is a log-log plot of the norm of the regularized solution versus the norm of the corresponding residual [29-30]. According to the L-curve results, the value of λ^2 is set to 5e-3.

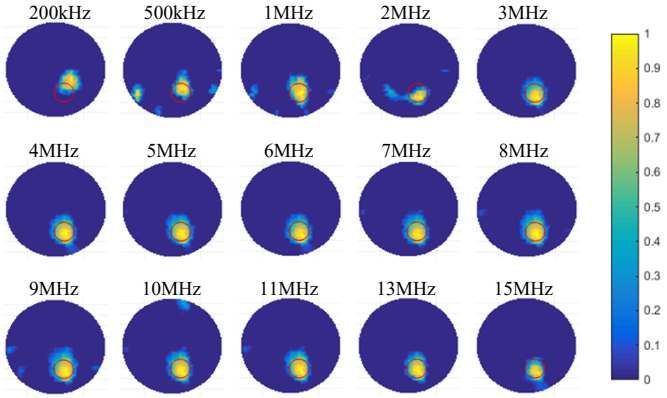

Fig. 11. Image reconstruction results of sample with the diameter of 35 mm.

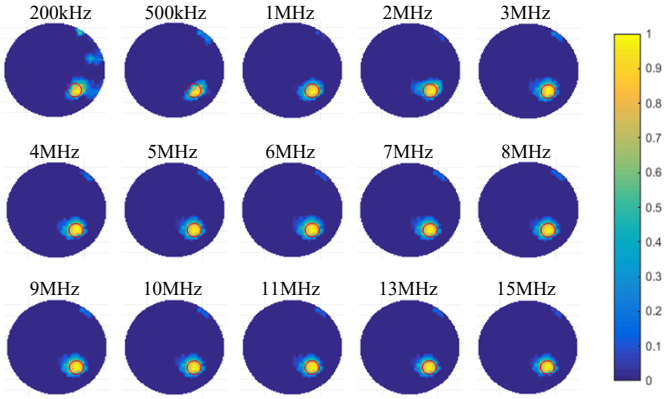

Fig. 12. Image reconstruction results of sample with the diameter of 25 mm.

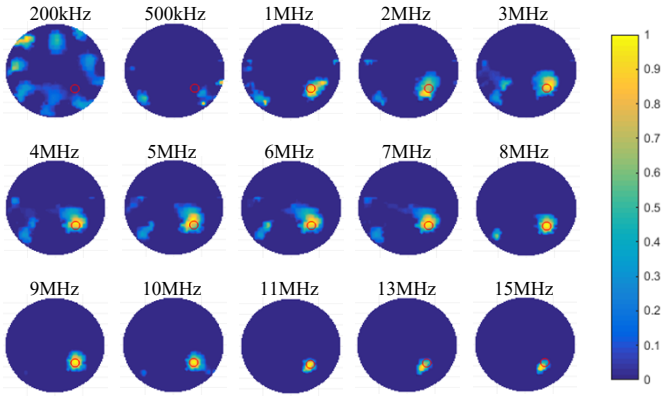

Fig. 13. Image reconstruction results of sample with the diameter of 15 mm.

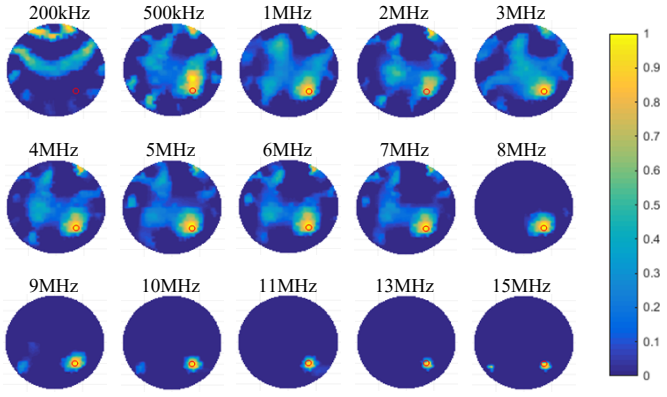

Fig. 14. Image reconstruction results of sample with the diameter of 10 mm.

From Fig. 11 to Fig. 14, we can see that for larger samples with the diameters of 35 mm and 25 mm, imaging results at the whole listed frequency range can provide good images of the samples. Besides, the images of larger samples are less noisy. However, for smaller samples with the diameters of 15 mm and 10 mm, as the change of measurements is smaller, the images are more vulnerable to noises. For the sample with diameter of 15 mm, at most frequencies above 1 MHz, good images can be reconstructed. While for the smallest sample with the diameter of 10 mm, a high frequency of at least 8 MHz can ensure good imaging results.

B. Discussion

In this work, effective simulation and experiments were carried out to study the safety and resolution of CCEIT for brain imaging. For simulation, an anatomically accurate but simplified head model is introduced and the simulation setup is consistent with the actual head structure. In the simplified head model, there are three subdomains, including the insulation layer which makes contactless measurement possible (the principle of CCEIT), the outer layer with low conductivity which represents the low-conductive layers of human head (i.e. the scalp and skull) and the brain layer which represents the higher conductive brain layer inside the human head. And for stroke patients, one more stroke layer is introduced into the brain layer. For practical experience, the insulation wall is the insulation layer, a very thin layer of glue painted on the internal face of the wall can be regarded as the low-conductive layers (almost non-conductive, i.e. the scalp and skull) and saline with the similar conductivity of brain layer is used to simulate the higher conductive brain layer. Besides, biomaterial sample (carrot sample) is introduced to simulate the stroke layer. As human tissue and carrot are both biomaterial samples, their models are similar, so the experiments are valid.

With the simulation results, it can be seen that for practical medical application, the safe excitation voltage of CCEIT equivalent to the standard excited EIT depends on many factors, such as the frequency and the thickness of the insulation layer. When a sensor is designed for practical application, the size of the sensing area and the insulation thickness are known, which means the allowable excitation voltage mainly depends on the highest working frequency.

In this work, the excitation signal is provided by Impedance Analyzer during the experiments. The amplitude of the voltage is 1 V. For the frequencies of 500 kHz and 15 MHz, the corresponding maximum total current density (norm) in the sensing area of 1 V excitation are respectively 0.0316 A/m^2 and 0.902 A/m^2, which is equivalent to an excitation current of 0.004 mA and 0.119 mA at 50 kHz for traditional EIT. That is much lower than the standard excitation of 1 mA at 50 kHz for traditional EIT, especially at low frequency. This may also be the reason of several phenomena observed from Fig. 11 ~ Fig. 14. First, the images are not very good when the frequency is low, and higher frequency can provide clearer images of the distribution in the sensing area. Second, for smaller samples, higher frequency is needed to obtain acceptable images because the signal at low frequency is too weak. In other words, the sample information is easier to be submerged by noise. Finally, increasing the frequency here is equivalent to enhancing the

excitation voltage, with the meaning of strengthening the electric field. It is necessary to point out that an excitation signal of 1 V at 15 MHz for CCEIT produces the same maximum total current density as that an excitation signal of 28.543 V at 500 kHz.

Although the resistance measurement has relatively good noise immunity, the low excitation voltage of the impedance analyzer makes the measurement still vulnerable to noises, especially in the central area of the phantom. That's why the samples in all the setups are close to the boundary (located at about 30 mm far from the insulation wall of the phantom) in this work. With the reference excitation level of this contactless CCEIT technique in mind, enhancing the voltage within the safety range can ensure better noise-to-signal ratio and can produce better images. In practical applications, researchers don't need to go so high in voltage amplitude at lower frequency, enough is the best.

In further vivo test or practical application, helmet sensor which embeds the electrodes into the helmet and has fixed insulation layer between patients' head and the electrodes can be designed. In our continued study, we will develop a custom made CCEIT device for stroke imaging. The level of voltage excitation to produce high enough changes in measurement data can be further simulated using forward model software.

This study shows a potential new imaging device for brain imaging, in particular for stroke detection and monitoring. CCEIT has great advantage of being contactless and compliment (as an alternative) to traditional EIT when it comes to frequencies higher than 1 MHz. The frequency range that CCEIT can operate is generally very challenging for traditional EIT, making it a very attractive alternative to cover the range of frequencies higher than 1 MHz. However, for very high frequency above 10 MHz, a slight position offset of the sample can be observed from the images in Fig. 11~14, which may be related to the forward modeling and shielding issues, making additional requirements on further complex modeling and necessary shielding.

For traditional EIT, similar-size electrodes with CCEIT could be problematic because large EIT electrodes will encourage currents to stay in the boundary and not go to depth of the head. So, usually small electrode size is preferred for EIT. As additional research, simulation work of EIT with the same electrode angle as CCEIT (24°) has also been undertaken. New EIT model was established and new electric field distribution can be obtained when excited again by the standard signal of 1 mA at 50 kHz, as shown in Fig. 15. As can be seen from the figure, the maximum total current density of EIT is 3.932 A/m^2. Similarly, the equivalent excitation levels of CCEIT that can produce the same level of maximum total current density can be obtained by simulation. The corresponding safe excitation references of CCEIT are respectively 124.359 V, 62.211 V, 12.621 V, 6.428 V and 4.359 V at 500 kHz, 1 MHz, 5 MHz, 10 MHz and 15 MHz. According to the research results with the same electrode sizes in EIT and CCEIT, similar conclusions can be made. Amplitude and frequency of the excitation signal are two closely related parts. As the frequency goes up, the excitation level should be reduced to ensure a safe level of electric field. But, by using space-filled electrodes, the maximum current density of EIT becomes smaller because the electric field is more dispersed. Although the equivalent safe reference of excitation level for CCEIT is lower in this case, there is still enough space to go for the CCEIT system in common frequency range (to select strong enough excitation signal for good performance, either by increasing excitation frequency or enhancing amplitude).

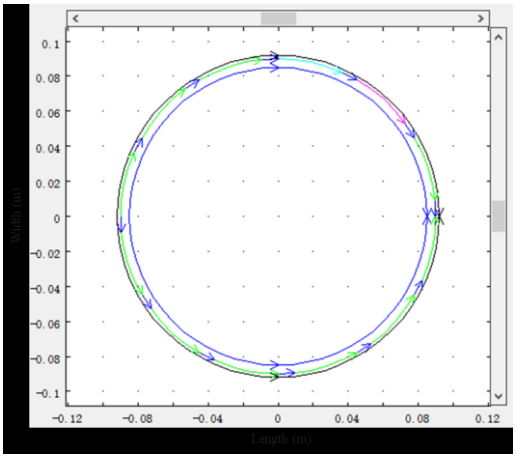

(a)

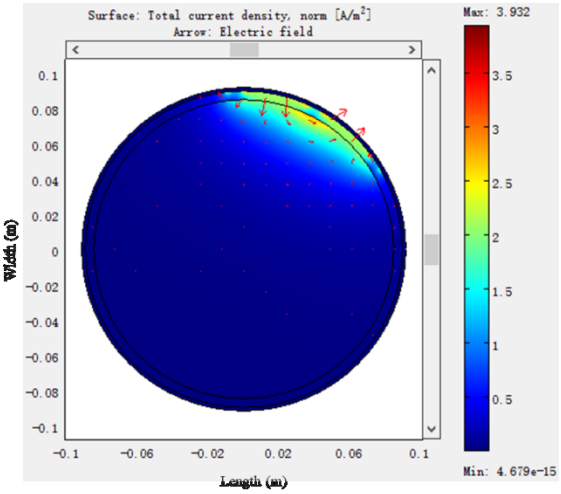

(b)

Fig. 15. Boundary setup and electric field distribution of EIT (electrode angle is 24°).

VII. Conclusion

This work introduces the new contactless CCEIT technique to medical imaging field for contactless measurement and studies various aspects of this technique for brain imaging. As the most critical point in medical application, safety issue of CCEIT in stroke imaging is considered and investigated when a comparative performance with traditional EIT is obtained. With the safe excitation reference of CCEIT in mind, it is easier to make a trade-off between safety and imaging quality. Experiments were carried out to investigate the resolution of this technique. Experimental results show that higher frequency is required to obtain good images of smaller sample, if the amplitude of the excitation voltage is very low. And although with the 1V excitation here, the images reconstructed at high

frequency can have a high resolution of 10 mm (the smallest detected sample in this work was 1/18 of the phantom size and was located at about 30 mm from the boundary). With higher allowable excitation level in CCEIT, even better performances are expected. The results of this paper offer an exciting new imaging technique that could have great implication for contactless and safe stroke imaging.

ACKNOWLEDGMENT

Financial support from China Scholarship Council (CSC) (No. 201706320268) is gratefully acknowledged.

REFERENCES

[1] A. Shehadah, G. M. Franklin and R. T. Benson. (2016, Aug.) Global disparities in stroke and why we should care. *Neurology*. 87(5), pp. 450-451.

[2] L. Yang, W. Liu, R. Chen, *et al.* (2017, Apr.) In Vivo Bioimpedance Spectroscopy Characterization of Healthy, Hemorrhagic and Ischemic Rabbit Brain within 10 Hz–1 MHz. *Sensors*. 17(4), 791.

[3] C. Tan, Y. Wu, Z. Xiao, *et al.* (2018, Jul.) Optimization of Dual Frequency-Difference MIT Sensor Array Based on Sensitivity and Resolution Analysis. *IEEE Access*. 6, pp. 34911-34920.

[4] L. Yang, M. Dai, C. Xu, *et al.* (2017, Jan.) The Frequency Spectral Properties of Electrode-Skin Contact Impedance on Human Head and Its Frequency-Dependent Effects on Frequency-Difference EIT in Stroke Detection from 10Hz to 1MHz. *PloS one*. 12(1), e0170563.

[5] T. Dowrick, C. Blochet and D. Holder. (2015, May) In vivo bioimpedance measurement of healthy and ischaemic rat brain: implications for stroke imaging using electrical impedance tomography. *Physiological measurement*. 36(6), pp. 1273-1282.

[6] F. Fu, B. Li, M. Dai, *et al.* (2014, Dec.) Use of electrical impedance tomography to monitor regional cerebral edema during clinical dehydration treatment. *Plos One*. 9(12), e113202.

[7] M. T. Clay and T. C. Ferree. (2002, Jun.) Weighted regularization in electrical impedance tomography with applications to acute cerebral stroke. *IEEE Transactions on Medical Imaging*. 21(6), pp. 629-637.

[8] A. McEwan, A. Romsauerova, R. Yerworth, *et al.* (2006, Apr.) Design and calibration of a compact multi-frequency EIT system for acute stroke imaging. *Physiological measurement*. 27(5), pp. S199-S210.

[9] B. McDermott, M. O'Halloran, E. Porter, *et al.* (2018, Jul.) Brain haemorrhage detection using a SVM classifier with electrical impedance tomography measurement frames. *PloS one*. 13(7), e0200469.

[10] X. E. Wei, J. Zhou, W. B. Li, *et al.* (2017, Jan.) MRI based thrombolysis for FLAIR-negative stroke patients within 4.5-6h after symptom onset. *Journal of the Neurological Sciences*. 372(15), pp. 421-427.

[11] J. B. Fiebach, P. D. Schellinger, O. Jansen, *et al.* (2002, Sep.) CT and diffusion-weighted MR imaging in randomized order: diffusion-weighted imaging results in higher accuracy and lower interrater variability in the diagnosis of hyperacute ischemic stroke. *Stroke*. 33(9), pp. 2206-2210.

[12] A. Mnyusiwalla, R. I. Aviv and S. P. Symons. (2009, Oct.) Radiation dose from multidetector row CT imaging for acute stroke. *Neuroradiology*, 51(10), pp. 635-640.

[13] R. Cardu, P. H. W. Leong and C. T. Jin. (2012, May) Electrode contact impedance sensitivity to variations in geometry. *Physiological measurement*. 33(5), pp. 817-830.

[14] V. Kolehmainen, M. Lassas, and P. Ola. (2008, Oct.) Electrical impedance tomography problem with inaccurately known boundary and contact impedances. *IEEE transactions on medical imaging*. 27(10), pp. 1404-1414.

[15] P. Hua, *et al*. (1993, Apr.) Finite Element Modeling of Electrode-Skin Contact Impedance in Electrical Impedance Tomography. *IEEE Transactions on Biomedical Engineering*. 40(4), pp. 335-343.

[16] T. Vilhunen, *et al*. (2002, Dec.) Simultaneous reconstruction of electrode contact impedances and internal electrical properties: I. Theory. *Measurement Science and Technology*. 13(12), pp. 1848-1854.

[17] B. Wang, *et al.* (2013, May) A novel electrical resistance tomography system based on C4D technique. *IEEE Transactions on Instrumentation and Measurement*. 62(5), pp. 1017-1024.

[18] B. Wang, *et al.* (2013, Jun.) Modeling and optimal design of sensor for capacitively coupled electrical resistance tomography system. *Flow Measurement and Instrumentation*. 31, pp. 3-9.

[19] Y. D. Jiang, M. Soleimani. (2018, May) Capacitively Coupled Resistivity Imaging for Biomaterial and Biomedical Applications. *IEEE Access*. 6, pp. 27069-27079.

[20] J. C. de Munck, T. J. C. Faes and R. M. Heethaar. (2000, Jun.) The boundary element method in the forward and inverse problem of electrical impedance tomography. *IEEE transactions on Biomedical Engineering*. 47(6), pp. 792-800.

[21] W. R. B. Lionheart. (2004, Feb.) EIT reconstruction algorithms: pitfalls, challenges and recent developments. *Physiological measurement*. 25(1), pp. 125-142.

[22] L. Borcea. (2002, Oct.) Electrical impedance tomography. *Inverse problems*. 18(6), pp. R99-R136.

[23] W. Q. Yang and L. H. Peng. (2003, Jan.) Image reconstruction algorithms for electrical capacitance tomography. *Measurement Science and Technology*. 14(1), Art. no. S0957-0233(03)39886-8.

[24] B. L. Wang, et al. (2017, Dec.) Image reconstruction algorithm for capacitively coupled electrical resistance tomography. *Flow Measurement and Instrumentation*. 40, pp. 216-222.

[25] V. Sarode, S. Patkar and A. N. Cheeran. (2013, May) Comparison of 2-D Algorithms in EIT based Image Reconstruction", *International Journal of Computer Applications*. 69(8), pp. 6-11.

[26] M. Vauhkonen, D. Vadasz, P. A. Karjalainen, *et al.* (1998, Apr.) Tikhonov regularization and prior information in electrical impedance tomography. *IEEE transactions on medical imaging*. 17(2), PP. 285-293.

[27] Z. Cui, et al. (2016, May) A review on image reconstruction algorithms for electrical capacitance/resistance tomography. *Sensor Review*. 36(4), pp. 429-445.

[28] M. Beister, D. Kolditz, W. A. Kalender. (1992, Dec.) Analysis of discrete ill-posed problems by means of the L-curve. *SIAM review*. 34(4), pp. 561-580.

[29] P. C. Hansen and D. P. O'Leary. (1993, Nov.) The use of the L-curve in the regularization of discrete ill-posed problems. *SIAM Journal on Scientific Computing*. 14(6), pp. 1487-1503.

[30] J. Avery, K. Aristovich, B. Low, *et al.* (2017, May) Reproducible 3D printed head tanks for electrical impedance tomography with realistic shape and conductivity distribution. *Physiological measurement*. 38(6), pp. 1116-1131.